

DOI: 10.1002/cctc.201402802

Continuous Flow Preparation of Iron Oxide Nanoparticles Supported on Porous Silicates

Alfonso Yopez,^[a] Frank L. Y. Lam,^[b] Antonio A. Romero,^[a] C. Oliver Kappe,^[c] and Rafael Luque^{*[a]}

A simple, innovative, and efficient continuous flow methodology for the direct preparation of supported nanoparticles on porous materials by using metal precursor solution flowing through heated packed-bed reactors containing the support material has been developed. The effects of the flow rate of the precursor solution, temperature, and nature of the support material and metal loading have been investigated. Results indicated that optimum conditions comprised short residence

times (with typical flow rates of 0.5 mL min⁻¹ and below) under mild heating (100 °C) to achieve optimum materials in terms of nanoparticle size and structure and catalytic activity. The support was found to have a remarkable effect on both loading and distribution and agglomeration of nanoparticles in the system, with a previously reported Fe/Al synergy also observed in the prepared nanomaterials, which led to optimum results.

Introduction

Heterogeneous metal supported catalysts have been widely studied for their potential applications in industrial chemical processes. Metal nanoparticles have attracted much attention in the past decade not only because of their relatively straightforward syntheses but owing to their applications in various important fields including catalysis.^[1,2] Several catalytic systems with different metal nanoparticles have been reported recently including supported catalysts containing gold,^[3,4] palladium,^[5,6] nickel,^[7] platinum,^[8] silver,^[9] cobalt,^[10] and copper.^[11]

Conventional preparations of metal nanoparticle catalysts including impregnation,^[3,12] coprecipitation,^[13] sol–gel processes,^[14] and deposition–precipitation^[15] have typically been conducted in a batch-mode operation. Promising alternative methodologies were reported in recent years to provide a number of designer nanomaterials for advanced catalytic applications under similar batch-mode conditions. These included protocols such as chemical vapor deposition,^[16] microwave-assisted synthesis,^[17] sonochemistry,^[18] photochemical deposition,^[19] and mechanochemistry (ball-milling).^[6,20] A scale-up process to streamline the production of nanomaterials and for whole-system efficiency is highly desirable. In this respect,

a simple and innovative approach that can meet the demands for high throughput coupled with a reduction in reagents and solvents involves continuous flow chemistry.

Continuous flow processes can provide a number of significant benefits for synthesis and reaction processing of nanomaterials compared to batch reactor technologies. Under continuous flow conditions, advantages including simplicity of preparation and operation, process control, flexibility, higher productivity, and controllable reaction conditions can be achieved easily to provide an alternative and comparatively practical approach for potential industrial scale-up syntheses compared to traditional protocols.^[21,22]

In light of the inherent advantages of continuous flow processes, particularly if related to nanomaterials syntheses,^[22,23] this work has been aimed at advancing the design of continuous flow synthetic protocols for the development of supported nanoparticles on porous supports. Herein, we report a simple, efficient, and innovative continuous flow preparation (CFP) of versatile Fe₂O₃ nanoparticles supported on porous aluminosilicates and their applications in acid (alkylation of toluene with benzyl chloride) and redox (oxidation of benzyl alcohol) catalyzed processes compared to analogous nanomaterials prepared by using other methods. Results from this work demonstrate the advantages of continuous-flow-synthesized nanomaterials in the selected chemistries over supported nanoparticles prepared under conventional impregnation deposition, microwave-assisted irradiation, and ball-milling.

Results and Discussion

Textural properties of synthesized materials in this work are summarized in Table 1. All materials exhibited high surface areas (> 700 m² g⁻¹), typical of mesoporous SBA-15 materials. The continuous flow incorporation of Fe into AlZn-SBA in-

[a] A. Yopez, Dr. A. A. Romero, Dr. R. Luque
Departamento de Universidad de Córdoba
Edificio Marie Curie, Ctra Nnal IV-A, Km 396, 14014, Córdoba (Spain)
E-mail: q62alsor@uco.es

[b] Dr. F. L. Y. Lam
Department of Chemical and Biomolecular Engineering
Hong Kong University of Science and Technology
Clear water bay, Kowloon (Hong Kong)

[c] Prof. C. O. Kappe
Institute of Chemistry
University of Graz
NAWI Graz, Heinrichstrasse 28, 8010 Graz (Austria)

 Supporting information for this article is available on the WWW under <http://dx.doi.org/10.1002/cctc.201402802>.

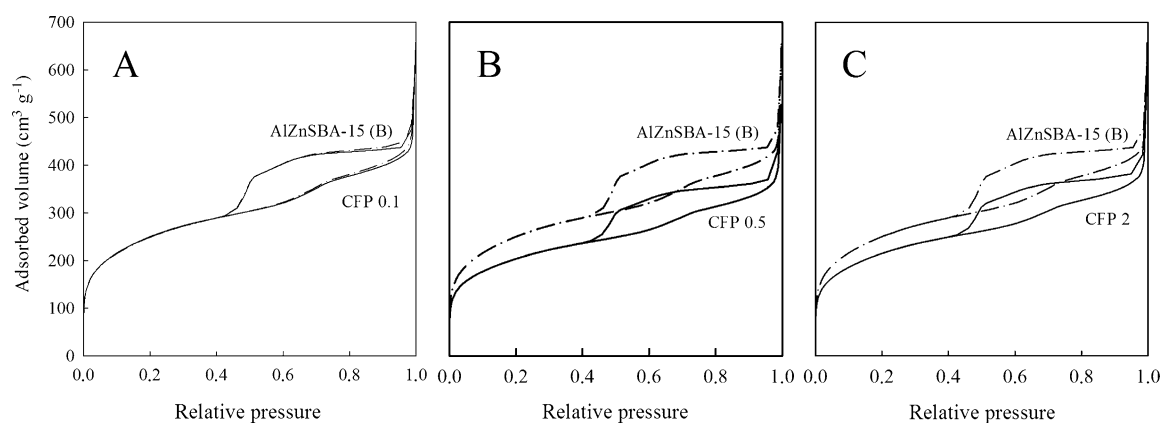


Figure 1. Isotherm profiles of Fe/AlZnSBA-15 materials prepared at different flow rates compared to parent AlZnSBA-15, [Si/(Al + Zn) = 20]. (B) denotes the parent support for this work.

duced a significant reduction in surface area but, interestingly, had little effect on pore sizes and volumes (Table 1). Pore sizes were in the range of 6 nm and remained almost unchanged upon Fe incorporation, particularly with reduced residence contact times (higher flow rate, 2 mL min⁻¹). Even at low iron loadings, these findings indicated a preferential surface deposition of supported Fe₂O₃ nanoparticles (reduction in surface area) with minor nanoparticle migration to the pores of the aluminosilicate support (unchanged pore sizes and volumes, no pore blocking upon Fe incorporation).^[24]

Isotherm profiles depicted in Figure 1 clearly illustrate the typical type IV profiles of mesoporous materials, in which the curves of CFP materials are almost identical to those of the parent supports.

The incorporation of Fe₂O₃ nanoparticles into AlZn-SBA did not significantly influence textural properties in Fe/AlZn-SBA except for surface areas. Wide-angle X-ray diffraction patterns show the typical amorphous nature of the aluminosilicate, with indications of Fe₂O₃ species in the materials (Figure 2).

These Fe₂O₃ species were confirmed by X-ray photoelectron spectroscopy analysis to be Fe³⁺ species (Figure 3), in good agreement with previous reports from Fe₂O₃ nanoparticles supported on similar aluminosilicates prepared by using different methods (e.g., microwave-assisted or mechanochemical deposition).^[25,26]

Inductively coupled plasma (ICP)-MS analysis indicated the stability of both Al and Zn at 100 °C upon Fe incorporation under continuous flow conditions and, most importantly, a generally good agreement with energy-dispersive X-ray spectroscopy (EDX) values for Fe content. With EDX considered a quasi-surface technique (penetration on the nm to 1–2 μm-scale), the results supported the previous observation of Fe species mostly present on the external surface of AlZn-SBA supports, with a relatively minor contribution within the pores evidenced for example in CFP0.1 (see the Experimental Section for a description of the notation used). In this material containing a larger Fe content, the differences between ICP-MS and EDX values for Fe content correlated well with a reduction in pore size and volume, clearly related to a migration of Fe species to the porous framework of the aluminosilicate.

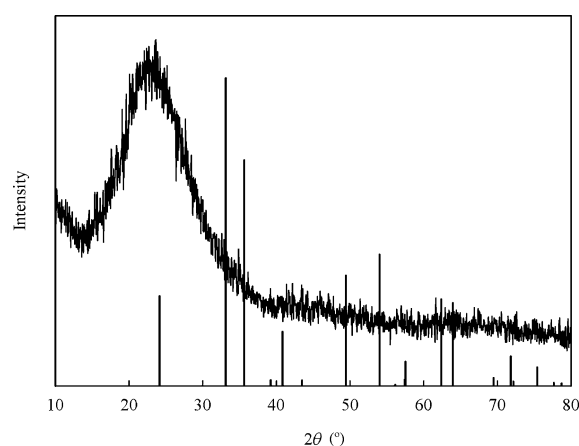


Figure 2. Wide-angle X-ray diffraction pattern of CFP0.1, showing a diffraction line at $2\theta = 23^\circ$ characteristic of amorphous silicates and incipient diffraction lines at $2\theta = 35$ and 37° corresponding to the diffraction pattern of the hematite Fe₂O₃ phase (Crystallography Open Database card number: 9000139).^[25,26]

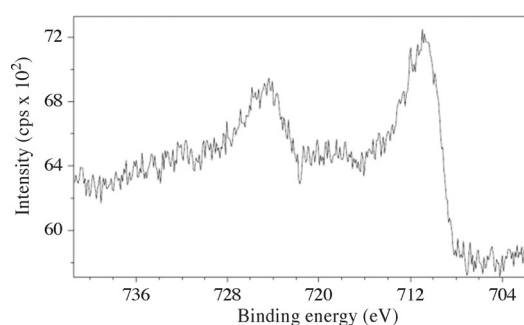


Figure 3. X-ray photoelectron spectra of CFP0.1, showing the distinctive major Fe³⁺ contributions at 710.8 eV (Fe 2p_{3/2}) and 724.0 eV (Fe 2p_{1/2}).^[26]

As expected, Fe content in the materials decreased at increasing flow rates (decreasing contact time between catalyst and ethanolic iron solution) but was generally under 1 wt% Fe, typically between 0.6 and 0.95 wt%. Fe-containing materials were highly reproducible between batches, exhibiting almost

identical textural properties and Fe contents. Although the catalyst structure and composition (e.g., nanoparticle size and distribution) may have varied spatially between the reactor inlet and outlet,^[27] we do not believe this was an important issue in the proposed microfluidic system, given the low metal loading and homogeneity of the synthesized materials. In previously reported cases, the use of a millifluidic chip could provide an in situ real-time analysis for a better understanding of the growth mechanism of gold nanostructures for catalytic applications.^[27]

These results confirmed the feasibility of the protocol in providing reproducible Fe contents in the materials under the investigated synthetic conditions. Further characterization by TEM proved the successful incorporation of Fe₂O₃ nanoparticles onto the mesoporous supports, shown clearly in Figure 4 (see also the Supporting Information). Fe₂O₃ nanoparticles were generally homogeneously dispersed in the aluminosilicate support, as clearly shown in TEM mapping of the different Fe/AlZn-SBA materials (Figure 5, see also the Supporting Information).

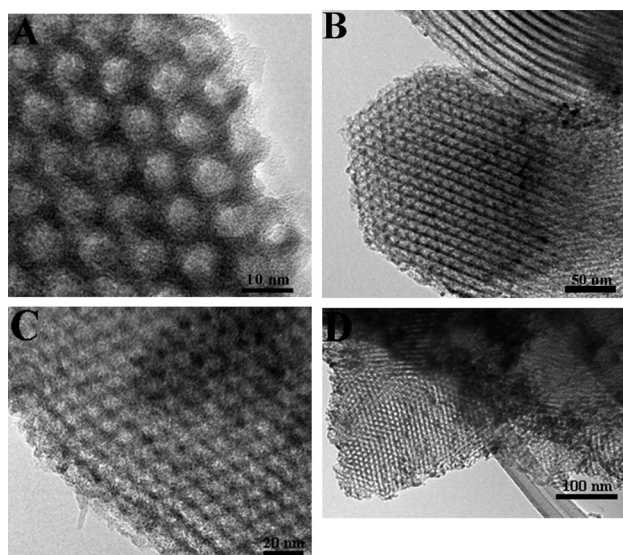


Figure 4. Representative TEM images at different magnifications of A) AlZn-SBA-15 support (showing mesopores ≈ 6.7 nm in size, see also Table 1), B) CFP0.1, C) CFP0.5, and D) CFP2 Fe₂O₃ nanoparticles supported on AlZn-SBA-15.

Synthesized Fe₂O₃ nanoparticle were typically spherical and in the 5–7 nm size range, with no remarkable changes in typical particle sizes for the majority of Fe₂O₃ nanoparticles at increasing flow rates (Figure 4B–D). The nanoparticle sizes of these nanomaterials were very similar to those reported previously.^[25,28,29] Nevertheless, an increasing number of inhomogeneities and clusters (nanoparticle aggregates, size > 20 nm) were clearly observed for materials prepared at increasing flow rates on the external surface of the materials (CFP2, Figures 4D and 6). These could have resulted partially from the proposed different compositions and structures of the materials between reactor inlet and outlet,^[27] although, as shown in Figures 4 and

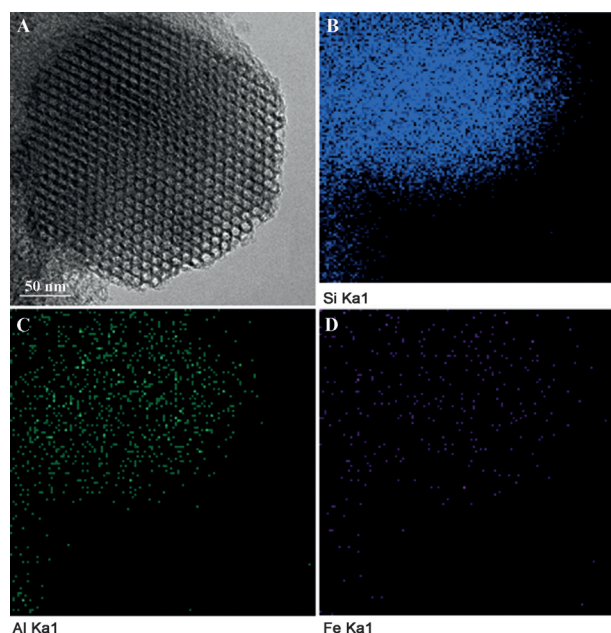


Figure 5. A) TEM image of CFP0.5 and corresponding mapping of B) Si, C) Al, and D) Fe elements, showing the excellent dispersion of Al and Fe and the absence of large Fe clusters in CFP supported Fe₂O₃ nanoparticles.

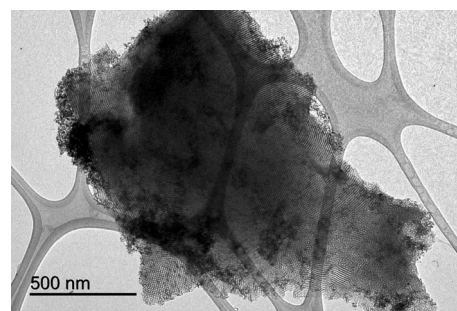


Figure 6. Larger Fe₂O₃ clusters and inhomogeneities in particle size distribution for selected areas in CFP2 materials.

5, agglomeration could not be considered significant for these particular systems (Fe and aluminosilicates) at flow rates under 1 mL min⁻¹.

The observation of Fe₂O₃ nanoparticles in the 5–7 nm size range also supported previous results on textural properties and consistent Fe content (ICP vs EDX) in a preferential deposition of Fe₂O₃ nanoparticles on the external surface of the materials with only minor migration of smaller nanoparticle (size < 6 nm) to the pores of the materials. Comparably, traditional impregnation–deposition methods resulted in the presence of nanoparticles both in the pores and on the external surface, whereas more advanced techniques (e.g., mechanochemical deposition) provided additional advantages in terms of a more controllable nanoparticle deposition and stabilization.

In view of the obtained results, flow rates below 1 mL min⁻¹, in particular between 0.1 and 0.5 mL min⁻¹, seemed to provide nanomaterials with optimum textural and structural properties. After characterization, the catalytic activities of the different CFP Fe-containing nanomaterials were tested in a range of het-

erogeneously catalyzed processes to illustrate the applicability and versatility of synthesized materials and to compare such activities with similar supported Fe_2O_3 nanoparticles prepared by using other synthetic protocols. Supported Fe_2O_3 nanoparticles were reported previously to be highly active and selective in oxidations^[25,28] and Lewis acid-catalyzed processes owing to the inherent Lewis acidity of Fe_2O_3 nanomaterials.^[25,29] Results of the catalytic activity of CFP nanomaterials in the microwave-assisted selective oxidation of benzyl alcohol are summarized in Table 2 and compared to previously reported similar Fe/Al-SBA-15 systems.

CFP iron-containing materials could reach conversions of 45–50% after 5 min of reaction, with high selectivities to benzaldehyde (>75%). Particularly good results were obtained with CFP2 (Fe/AlZn-SBA, flow rate 2 mL min^{-1}) in terms of conversion and selectivity to benzaldehyde, which indicated the reaction was not nanoparticle-size-sensitive. Comparatively, analogous type of materials synthesized by using the conventional wetness impregnation technique (IMP-Fe/AlZnSBA, Tables 2 and 3) could reach a maximum conversion of 26% (98% selectivity to benzaldehyde) under identical reaction conditions. Even Fe-based systems prepared by using advanced methodologies including microwave-assisted deposition (MW-Fe/AlZnSBA, Tables 2 and 3) and mechanochemical dry ball-milling (BM-Fe/AlZnSBA, Tables 2 and 3) provided comparable activities under identical conditions (conversions of typically 40–45%), illustrating the outstanding catalytic activities of the CFP nanomaterials.

Fe-containing aluminosilicates were subsequently explored in the microwave-assisted alkylation of toluene with benzyl chloride (Table 3). For this particular process, results showed a remarkable increase in activity for CFP nanomaterials (88–99% conversion) compared to conventional impregnation, microwave, and even mechanochemical ball-milling-synthesized catalysts under otherwise identical reaction conditions. Quantitative conversion of starting material was observed for CFP0.1 and CFP2, which was a significant improvement on the typical 40–65% conversion achieved previously for Fe-containing materials under identical reaction conditions. Although further investigations are required to better understand the influence of the electronic structure on catalytic activity in the systems,^[30,31] the proposed system has potential to provide access to a wide range of advanced nanomaterials for catalytic applications in a very simple and straightforward way.

Stability and reusability of CFP nanomaterials were also investigated in the key microwave-assisted processes. Iron-containing nanomaterials were deactivated gradually after each use, with improved catalytic activities only after regeneration of the materials upon calcination (Figure 7). The most plausible explanation for the quick deactivation relates to the poisoning of highly accessible active sites on the external surface of the support. After calcination and surface cleaning, the materials showed similar catalytic performances to those of the fresh catalysts. Selectivities in both reactions were similar after each reuse, with the exception of an increase in selectivity to benzaldehyde (>90%) after two uses in the selective oxidation of benzyl alcohol. In all cases, no significant Fe leaching into solu-

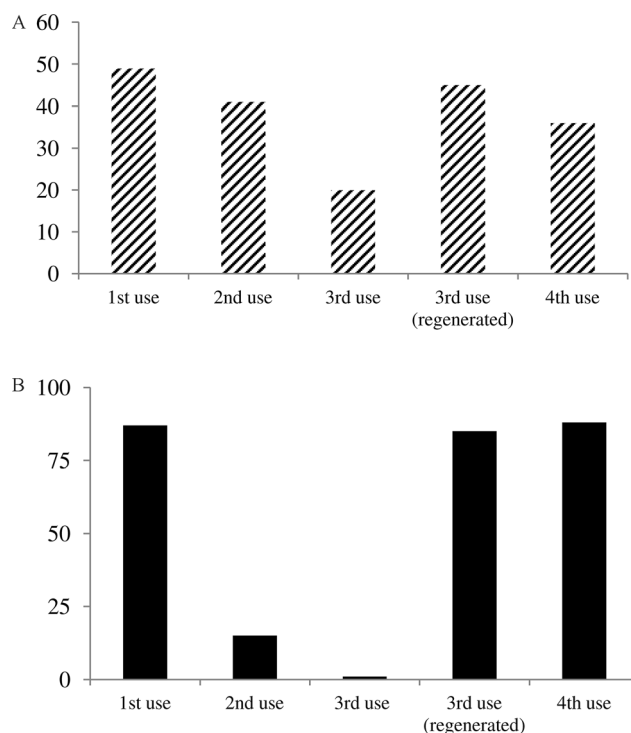


Figure 7. Reuses of CFP0.5 in the microwave-assisted A) oxidation of benzyl alcohol and B) alkylation of toluene with benzyl chloride (for reaction conditions, see Tables 2 and 3, respectively).

tion was observed in most cases, in good agreement with previous reports.^[32,25,28] Only in the case of the alkylation reaction (Figure 7B) was significant deactivation observed in the second and third use that was due partly to the removal of weakly physisorbed or deposited Fe species (some Fe was observed in solution), owing to the generation of HCl as a byproduct of the reaction of benzyl chloride. Upon regeneration, the catalytic activity was recovered owing to a combination of the activity of Fe_2O_3 nanoparticles and oxychloride species generated in the materials, similar to that reported previously for analogous Zr-SBA-15 materials.^[33]

Conclusions

A continuous flow synthesis of supported nanoparticles on porous materials was reported. Featuring simplicity, efficiency, better process control, and the possibility of scaling up the synthesis to the multigram-scale, the synthesized supported Fe_2O_3 nanomaterials possessed a remarkable activity and versatility in selective oxidation (benzyl alcohol to benzaldehyde) and acid-catalyzed processes (alkylation of toluene and cetyl alcohol dehydration). A comparison of these nanomaterials prepared in continuous flow with previously reported literature catalysts clearly indicated the comparable, if not superior activities of the continuous-flow-prepared catalysts compared to materials prepared by using microwave-assisted or mechanochemical techniques, which illustrated the potential of the proposed methodology for the preparation of designer nanocatalysts for advanced catalytic processes, including biomass valori-

zation (i.e., palm oil waste hydrogenation to fatty alcohols and subsequent dehydration) and room temperature catalysis, currently under investigation in our laboratories.

Experimental Section

Materials synthesis

Synthesis of AlZn-SBA-15 [Si/(Al+Zn) = 20]

The synthesis of AlZn-SBA-15 materials was reported previously.^[32] In brief, the required quantity of zinc acetate (0.443 g) was added to a typical synthesis gel for an Al-SBA-15 synthesis protocol to achieve a theoretical Si/(Al+Zn) ratio of 20 in the final material. Upon Zn addition, the gel was aged typically at 100 °C for 24 h. The final material was then filtered off, dried overnight at RT, and calcined in a N₂ atmosphere at 600 °C for 2 h, then in air for an additional 6 h. Zn content in AlZn-SBA was measured to be approximately 0.2 wt% by using ICP-MS (Table 1).

Continuous flow synthesis of supported Fe₂O₃ nanoparticles on AlZn-SBA-15

The continuous flow deposition of Fe₂O₃ nanoparticles on AlZn-SBA was performed under a series of conditions by using an innovative continuous flow setup depicted in Figure 8. A stainless-steel reactor (1.2 cm³ volume) was packed with AlZn-SBA support (typically 0.5 g) set between two plugs of quartz wool to prevent the solid support from moving in the reactor upon pumping in the flow of the solution of the metal precursor. Separately, a 0.5 wt% Fe solution in ethanol was prepared by using FeCl₂·4H₂O (0.89 g in 50 mL ethanol) as the Fe precursor. The solution was filtered off prior to flowing it through the system to prevent the presence of any undissolved metal precursor. The system started with pumping a solution of pure ethanol (0.5 mL min⁻¹, 5 min) through the catalyst bed to wet the catalyst. The temperature of the reactor was

Table 1. Textural properties and ICP-MS analysis of mesoporous aluminosilicates synthesized in this work.

Material	Surface area ^[a] [m ² g ⁻¹]	Pore size [nm]	Pore volume ^[b] [mL g ⁻¹]	Elemental composition ^[c] [%]		
				Fe ^[d]	Al	Zn
AlZn-SBA	901	6.7	0.37	–	0.30	0.02
CFP0.1	769	6.2	0.33	0.95 (0.76)	0.28	0.02
CFP0.5	729	6.4	0.34	0.65 (0.79)	0.27	0.01
CFP2	773	6.6	0.33	0.61 (0.59)	0.24	0.02

[a] BET surface area was estimated by using a multipoint BET method with adsorption data in the relative pressure range of 0.05–0.30. [b] Mesopore volume was calculated from the isotherm data by using the DFT method, otherwise pore volume was calculated from the isotherm data at a relative pressure of 0.95. [c] Based on ICP-MS and EDX analyses. [d] EDX values in parentheses as an average of three measurements.

then set to 100 °C and the system changed to the 0.5 wt% Fe solution, which was pumped through the system at different flow rates. The incorporation was conducted at three different flow rates (0.1, 0.5, and 2 mL min⁻¹) and different times (60, 15, and 10 min, respectively) to compare results and residence times. At the end of the continuous flow process, the system was switched to ethanol, which was pumped through the Fe-incorporated catalyst at 100 °C to remove physisorbed and unreacted Fe species on

Table 2. Microwave-assisted oxidation of benzyl alcohol with different mesoporous aluminosilicates.^[a]

Material	Conversion [mol %]	Selectivity [mol %]	
		Benzaldehyde	Benzoic acid
AlZn-SBA (B)	< 10	100	–
CFP0.1	44	93	7
CFP0.5	51	75	25
CFP2	50	87	13
IMP-Fe/AlZnSBA ^[25c]	26	98	2
MW-Fe/AlZnSBA ^[25c]	42	85	15
BM-Fe/AlZnSBA ^[25c]	44	90	10

[a] Reaction conditions: 0.2 mL benzyl alcohol, 0.3 mL H₂O₂ 50% (v/v), 2 mL acetonitrile, 0.05 g catalyst, 300 W, 5 min.

Table 3. Microwave-assisted alkylation of toluene with benzyl chloride with different mesoporous aluminosilicates.^[a]

Material	Conversion [mol %]	Selectivity [mol %]		
		<i>ortho</i>	<i>meta</i>	<i>para</i>
AlZn-SBA (B)	< 5	42	10	48
CFP0.1	> 99	44	9	47
CFP0.5	88	44	9	47
CFP2	96	48	5	46
IMP-Fe/Al-SBA ^[29]	38	42	10	48
MW-Fe/Al-SBA ^[29]	60	45	8	47
BM-Fe/Al-SBA ^[29]	45	46	5	49

[a] Reaction conditions: 2 mL toluene, 0.2 mL benzyl chloride, 0.025 g catalyst, 300 W, 120 °C, 3 min.

the catalyst. Materials were then recovered from the reactor, ground with a pestle and mortar, and subsequently oven-dried at 100 °C. Final materials were calcined at 400 °C for 4 h under air. Fe/AlZn-SBA materials were denoted as CFP_x, in which *x* represented the flow rates of 0.1, 0.5, or 2 mL min⁻¹ used during the incorporation process over 60, 15, or 8 min, respectively, at 100 °C with a 0.5 wt% theoretical loading of Fe. Samples were highly reproducible from batch to batch.

Materials characterization

Materials were characterized by using N₂ physisorption, powder X-ray diffraction, TEM, and ICP-MS analyses.

N₂ adsorption measurements were performed at 77 K by using an Micromeritics ASAP 2000 volumetric adsorption analyzer. The samples were outgassed for 24 h at 100 °C under vacuum (*P*₀ = 10⁻² Pa) and subsequently analyzed. The linear part of the BET equation (relative pressure 0.05–0.30) was used for the determination of the specific surface area. Mean pore size diameter and pore volumes were obtained from porosimetry data by using the BJH method.

Wide-angle X-ray diffraction experiments were recorded on a PanAnalytic/Philips X'pert MRD diffractometer (40 kV, 30 mA) with



Figure 8. Experimental setup for the continuous flow preparation of Fe/AlZn-SBA materials.

CuK_α ($\lambda = 0.15418$ nm) radiation. Scans were performed over a $2\theta = 10\text{--}80^\circ$ at step size of 0.018° with a counting time per step of 5 s. TEM images of the samples were obtained on JEM 2010F (JEOL) and Phillips Analytical FEI Tecnai 30 microscopes.

X-ray photoelectron spectroscopy was performed with a Kratos Analytical AXIS 165 electron spectrometer with a monochromated AlK_α X-ray source run at 100 W. Survey scans were taken with a 1.0 eV step and 80 eV analyzer pass energy and the high resolution regional spectra were recorded with a 0.1 eV step and 20 eV pass energy. The base pressure was typically 133 nPa.

The metal content in the materials was determined by using ICP in a Philips PU 70000 sequential spectrometer equipped with an Echelle monochromator (0.0075 nm resolution) and coupled to a mass spectrometer. Samples were digested in HNO_3 and subsequently analyzed by using ICP-MS at the SCAI of Universidad de Córdoba.

Catalytic experiments

Microwave-assisted selective oxidation of benzyl alcohol

Typical procedure: benzyl alcohol (0.2 mL), H_2O_2 (50% v/v, 0.3 mL), acetonitrile (2 mL), and catalyst (25 mol%, 0.15–0.25 mol% Fe, 0.05 g) were added to a Pyrex vial and radiated with microwaves in a pressure-controlled CEM-Discover microwave reactor for 5 min at 300 W maximum power output ($T_{\text{max}} = 120\text{--}125^\circ\text{C}$, $P_{\text{max}} = 1.65$ MPa) under continuous stirring. Samples were then withdrawn from the reaction mixture and analyzed by using GC on an Agilent 6890N fitted with a capillary column HP-5 (30 m \times 0.32 mm \times 0.25 m) and a flame ionization detector. The identity of the products was confirmed by GC-MS. Microwave experiments were conducted in closed-vessel mode, generally temperature-controlled (by using an infra-red probe), in which the samples were irradiated with the required power output (maximum power setting: 300 W) to achieve the desired temperature.

Microwave-assisted alkylation of toluene with benzyl chloride

Typical procedure: toluene (2 mL), benzyl chloride (0.2 mL) and catalyst (11 mol%, 0.07–0.1 mol% Fe, 0.025 g) were added to a Pyrex vial and microwaved in a pressure-controlled CEM-Discover micro-

wave reactor for 3 min at 300 W ($T_{\text{max}} = 110\text{--}120^\circ\text{C}$) under continuous stirring. Samples were then withdrawn from the reaction mixture and analyzed in a similar way to that reported above. Microwave experiments were in this case run in open-vessel mode due to the presence of HCl as reaction by-product.

Acknowledgements

R.L. gratefully acknowledges Spanish MICINN for financial support via the concession of a RyC contract (ref: RYC-2009-04199) and funding under project CTQ2011-28954-C02-02 (MEC). Consejería de Ciencia e Innovación, Junta de Andalucía is also gratefully acknowledged for funding project P10-FQM-6711. The authors are deeply indebted to both reviewers of the manuscript for their useful suggestions and comments to improve its quality and standards.

Keywords: continuous flow systems • iron • mesoporous materials • nanoparticles • silicates

- [1] B. C. Gates, *Chem. Rev.* **1995**, *95*, 511.
- [2] C. L. Geiger, K. Carvalho-Knighton, S. Novaes-Card, P. Maloney, R. A. Devor, *Environmental Applications of Nanoscale and Microscale Reactive Metal Particles, Chapter 1*, ACS Symposium Series **2010**, 1027, 1.
- [3] A. Pineda, L. Gomez, A. M. Balu, V. Sebastian, M. Ojeda, M. Arruebo, A. A. Romero, J. Santamaria, R. Luque, *Green Chem.* **2013**, *15*, 2043.
- [4] N. K. Gupta, S. Nishimura, A. Takagaki, K. Ebitani, *Green Chem.* **2011**, *13*, 824.
- [5] a) S. A. Kondrat, G. Shaw, S. J. Freakley, Q. He, J. Hampton, J. K. Edwards, P. J. Miedzkiak, T. S. E. Davies, A. F. Carley, S. H. Taylor, C. J. Kiely, G. J. Hutchings, *Chem. Sci.* **2012**, *3*, 2965; b) A. R. Siamaki, Y. Lin, K. Woodberry, J. W. Connell, B. F. Gupton, *J. Mater. Chem. A* **2013**, *1*, 12909; c) R. Zhang, A. Villanueva, H. Alamdari, S. Kaliaguine, *J. Catal.* **2006**, *237*, 368; d) R. Zhang, H. Alamdari, S. Kaliaguine, *Appl. Catal. A* **2008**, *340*, 140.
- [6] M. Ojeda, A. Pineda, A. A. Romero, V. Barron, R. Luque, *ChemSusChem* **2014**, *7*, 1876.
- [7] H. Y. Wang, A. C. Lua, *J. Phys. Chem. C* **2012**, *116*, 26765.
- [8] B. M. Quinn, C. Dekker, S. G. Lemay, *J. Am. Chem. Soc.* **2005**, *127*, 6146.
- [9] T. M. Day, P. R. Unwin, N. R. Wilson, J. V. Macpherson, *J. Am. Chem. Soc.* **2005**, *127*, 10639.
- [10] Y.-T. Tsai, X. Mo, A. Campos, J. G. Goodwin, J. J. Spivey, *Appl. Catal. A* **2011**, *396*, 91.
- [11] F. L. Y. Lam, A. C. K. Yip, X. Hu, *Ind. Eng. Chem. Res.* **2007**, *46*, 3328.
- [12] S. M. Choi, M. H. Seo, H. J. Kim, W. B. Kim, *Synth. Met.* **2011**, *161*, 2405.
- [13] D. Horváth, L. Toth, L. Guzzi, *Catal. Lett.* **2000**, *67*, 117.
- [14] J. Liu, S. Zou, S. Li, X. Liao, Y. Hong, L. Xiao, J. Fan, *J. Mater. Chem. A* **2013**, *1*, 4038.
- [15] A. Sandoval, A. Gomez-Cortes, R. Zanella, G. Diaz, J. M. Saniger, *J. Mol. Catal. A* **2007**, *278*, 200.
- [16] F. L. Y. Lam, T. C. Y. Martin, X. Hu, *Chem. Commun.* **2008**, 6390.
- [17] a) G. Glaspell, L. Fuoco, M. S. El-Shall, *J. Phys. Chem. B* **2005**, *109*, 17350; b) Z. Lui, X. Y. Ling, B. Guo, L. Hong, J. Y. Lee, *J. Power Sources* **2007**, *167*, 272; c) J. M. Campelo, T. D. Conesa, M. J. Gracia, M. J. Jurado, R. Luque, J. M. Marinas, A. A. Romero, *Green Chem.* **2008**, *10*, 853.
- [18] a) J. C. Colmenares, *ChemSusChem* **2014**, *7*, 1512; b) J. C. Colmenares, A. Magdziarz, O. Chernyayeva, D. Lisovtyskiy, K. Kurzydowski, J. Grzonka, *ChemCatChem* **2013**, *5*, 2270; c) J. C. Colmenares, A. Magdziarz, K. Kurzydowski, J. Grzonka, O. Chernyayeva, D. Lisovtyskiy, *Appl. Catal. B* **2013**, *134–135*, 136.
- [19] J. C. Colmenares, A. Magdziarz, D. Łomot, O. Chernyayeva, D. Lisovtyskiy, *Appl. Catal. B* **2014**, *147*, 624.
- [20] a) Y. Lin, K. A. Watson, M. J. Fallbach, S. Ghose, J. G. Smith, D. M. Delozier, W. Cao, R. E. Crooks, J. W. Connell, *ACS Nano* **2009**, *3*, 871; b) M. J. Rak, N. K. Saadé, T. Frišćić, A. Moores, *Green Chem.* **2014**, *16*, 86; c) M. J. Rak, T. Friscic, A. Moores, *Faraday Discuss.* **2014**, *170*, 155–167.

- [21] For recent reviews on continuous flow synthesis of nanomaterials, see: a) Y. Song, J. Hormes, C. S. S. R. Kumar, *Small* **2008**, *4*, 698; b) S. Marre, K. F. Jensen, *Chem. Soc. Rev.* **2010**, *39*, 1183; c) C.-X. Zhao, L. He, S. Z. Qiao, A. P. Middelberg, *Chem. Eng. Sci.* **2011**, *66*, 1463; d) M. Pumera, *Chem. Commun.* **2011**, *47*, 5671.
- [22] For recent examples from our laboratories, see: a) M. Mirhosseini Moghaddam, B. Pieber, T. Glasnov, C. O. Kappe, *ChemSusChem* **2014**, *7*, 3122–3131; b) D. Cantillo, M. Baghbanzadeh, C. O. Kappe, *Angew. Chem. Int. Ed.* **2012**, *51*, 10190; *Angew. Chem.* **2012**, *124*, 10337; c) M. Mirhosseini Moghaddam, M. Baghbanzadeh, A. Sadeghpour, O. Glatter, C. O. Kappe, *Chem. Eur. J.* **2013**, *19*, 11629; d) M. Baghbanzadeh, T. N. Glasnov, C. O. Kappe, *J. Flow Chem.* **2013**, *3*, 109.
- [23] E. Shahbazali, V. Hessel, T. Noel, Q. Wang, *Nanotechnol. Rev.* **2014**, *3*, 65–86.
- [24] For a related continuous flow loading of Pd nanoparticles onto monolithic materials, see: K. Mennecke, R. Cecilia, T. N. Glasnov, S. Gruhl, C. Vogt, A. Feldhoff, M. A. L. Vargas, C. O. Kappe, U. Kunz, A. Kirschning, *Adv. Synth. Catal.* **2008**, *350*, 717 and references cited therein.
- [25] a) A. Pineda, A. M. Balu, J. M. Campelo, A. A. Romero, D. Carmona, F. Balas, J. Santamaria, R. Luque, *ChemSusChem* **2011**, *4*, 1561; b) A. Mariana Balu, A. Pineda, K. Yoshida, J. M. Campelo, P. L. Gai, R. Luque, A. A. Romero, *Chem. Commun.* **2010**, *46*, 7825.
- [26] a) *Handbook of X-Ray Photoelectron Spectroscopy* (Eds.: C. D. Wagner, W. N. Riggs, L. E. Davis, G. F. Moulder, G. E. Muilenberg), PerkinElmer, Eden Prairie, **1979**; b) X. Deng, J. Lee, D. Matranga, *Surf. Sci.* **2010**, *604*, 627.
- [27] K. Sai Krishna, C. V. Navin, S. Biswas, V. Singh, K. Ham, G. L. Bovenkamp, C. S. Theegala, J. T. Miller, J. J. Spivey, C. S. S. R. Kumar, *J. Am. Chem. Soc.* **2013**, *135*, 5450.
- [28] a) F. Rajabi, A. Pineda, S. Nahresian, A. M. Balu, A. A. Romero, R. Luque, *Green Chem.* **2013**, *15*, 1232; b) F. Rajabi, N. Karimi, M. Reza Saidi, A. Primo, R. S. Varma, R. Luque, *Adv. Synth. Catal.* **2012**, *354*, 1707; c) A. M. Balu, C. S. K. Lin, H. Liu, C. Vargas, Y. Li, R. Luque, *Appl. Catal. A* **2013**, *455*, 261.
- [29] A. Pineda, A. M. Balu, J. M. Campelo, R. Luque, A. A. Romero, J. C. Serrano-Ruiz, *Catal. Today* **2012**, *187*, 65.
- [30] R. Jin, *Nanotechnol. Rev.* **2012**, *1*, 31.
- [31] H. Li, L. Li, Y. Li, *Nanotechnol. Rev.* **2013**, *2*, 515.
- [32] A. Yepez, A. Pineda, A. Garcia, A. A. Romero, R. Luque, *Phys. Chem. Chem. Phys.* **2013**, *15*, 12165.
- [33] M. D. Gracia, A. M. Balu, J. M. Campelo, R. Luque, J. M. Marinas, A. A. Romero, *Appl. Catal. A* **2009**, *371*, 85.

Received: October 8, 2014

Revised: October 17, 2014

Published online on ■ ■ ■, 0000

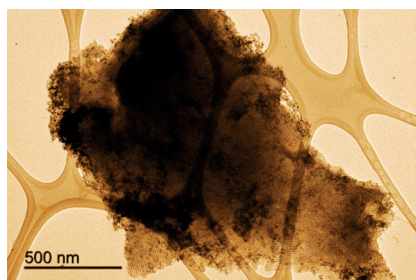
FULL PAPERS

A. Yepez, F. L. Y. Lam, A. A. Romero,
C. O. Kappe, R. Luque*

■ ■ - ■ ■



**Continuous Flow Preparation of Iron
Oxide Nanoparticles Supported on
Porous Silicates**



Nanoparticles in full flow: Nanoparticles supported on porous materials are prepared directly in continuous flow by using a metal precursor solution flowing through heated packed-bed reactors that contain the support material. The support affects nanoparticle loading, distribution, and agglomeration in the system, with an Fe/Al synergy that leads to optimum results.
